BMC Microbiology

RESEARCH

Open Access

6-thioguanine inhibits EV71 replication by reducing BIRC3-mediated autophagy

Qiao You[1†], Jing Wu[1,2†], Ruining Lyu[1], Yurong Cai[3], Na Jiang[1], Ye Liu[4], Fang Zhang[5], Yating He[1], Deyan Chen[1,6,8*] and Zhiwei Wu[1,7,8*]

Abstract

Background Enterovirus 71 (EV71) is one of the major causative agents of hand, foot, and mouth disease (HFMD), and can cause severe cerebral complications and even fatality in children younger than 5 years old. However, there is no specific medication for EV71 infection in clinical practice. Our previous studies had identified the 6-thioguanine (6-TG), an FDA-approved anticancer drug, as a potential antiviral agent, but its anti-EV71 activity is largely unknown, therefore, we aim to explore the antiviral effect of 6-TG on EV71.

Results 6-TG significantly suppressed EV71 mRNA level, VP1 protein expression, and viral progeny production in HT-29 cells. In EV71-infected HT-29 cells, the 50% cytotoxicity concentration of 6-TG (CC_{50}) was > 2000 μM and the 50% inhibitory concentration of 6-TG against EV71 (IC_{50}) was 0.9302 μM. Interestingly, the selectivity index (SI) value of 6-TG against EV71 was > 2150.1, which was higher than the SI value (> 66.7) of ribavirin. Mechanistically, 6-TG treatment reduced the expression of baculoviral IAP repeat containing 3 (BIRC3), and further inhibited EV71 replication by attenuating BIRC3-mediated the complete autophagy.

Conclusions 6-TG exerted a significant inhibitory effect on EV71 infection in vitro and prevented EV71-induced the complete autophagy by decreasing BIRC3 expression. Our work provided a basis for the further development of 6-TG as a therapy for EV71-associated HFMD.

Keywords 6-thioguanine (6-TG), EV71, BIRC3, Autophagy

†Qiao You and Jing Wu contributed equally to this work.

*Correspondence:
Deyan Chen
chendeyan@nju.edu.cn
Zhiwei Wu
wzhw@nju.edu.cn
[1]Center for Public Health Research, Medical School of Nanjing University, Nanjing, China
[2]Department of Preventive Medicine, School of Public Health, Fujian Medical University, Fuzhou, China
[3]Ningxia Institute of Clinical Medicine, Central Laboratory, People's Hospital of Ningxia Hui Autonomous Region, Ningxia Medical University, Yinchuan, China
[4]China Department of Ophthalmology, Tianjin First Central Hospital, Tianjin, China
[5]Department of Burn and Plastic Surgery, Affiliated Hospital of Zunyi Medical University, Zunyi, China
[6]Key Laboratory of Infection and Immunity of Anhui Higher Education Institutes, Bengbu Medical University, 2600 Donghai Avenue, Bengbu, Anhui, China
[7]State Key Laboratory of Analytical Chemistry for Life Science, Nanjing University, Nanjing, China
[8]Medical School of Nanjing University, Nanjing 210093, China

Background

Hand, foot and mouth disease (HFMD) has become a seasonal infectious disease among children (under 5 years old) in the summer and fall in the Asia-Pacific region [1, 2]. Enterovirus 71 (EV71), a non-enveloped, positive-sense, single-stranded RNA virus in the family *Picornaviridae*, is the major causative agent of HFMD [3]. HFMD cases often present symptoms of small red herpes on the hands, foot and mouth. Though HFMD is mostly self-limiting, a small proportion of cases even develop severe complications such as acute encephalitis, acute flaccid paralysis, pulmonary edema, cardiorespiratory complication, and death [4]. Although inactivated vaccines have been licensed in China with a high efficacy (90–97.4%) against EV71–associated HFMD [5–7], they offered the limited protection against the other genotypes of EV71 due to the fact that vaccines were mostly developed based on a single serotype strain C4 [8, 9]. A therapeutic drug for EV71 is not yet available, therefore, it is necessary to investigate the potential agents with anti-EV71 activity.

6-thioguanine (6-TG), a thiopurine drug, was approved by US Food and Drug Administration (FDA) for the treatment of childhood leukemia in 1950s [10]. Nowadays, 6-TG was more widely used in the treatment of chronic inflammatory diseases including inflammatory bowel disease (IBD) and psoriasis [11]. In addition to the anti-cancer and anti-inflammatory effect, 6-TG also exhibited antiviral activities against the severe acute respiratory syndrome coronavirus 2 (SARS-COV-2) and influenza A virus [12, 13]. Moreover, our previous studies have reported that 6-TG inhibited the severe fever with thrombocytopenia syndrome virus (SFTSV) and Herpes Simples Virus 1 (HSV-1) infection [14, 15]. However, the roles of 6-TG on EV71 infection are not fully understood.

Autophagy is an essential pathway to maintain cellular homeostasis by constituting the catabolic process of misfold proteins, degradation of damaged organelle, and defense against harmful microbes [16]. The process of autophagy begins with the formation of crescent-shaped membrane structures known as phagophore, which expands to form a closed double-membrane vesicle with the transform of LC3 I (MAP1LC3B, microtubule associated protein 1 light chain 3 beta) to the lipoylated LC3 II, called autophagosome. The autophagosome then fuses with a lysosome, and the cargoes in the autophagosome are digested by lysosomal enzymes for recycling [17]. Many viruses including EV71 induce autophagy with observed GFP-LC3 puncta and increased lipid-bound LC3 II level in vivo and in vitro, and EV71 might hijack the autophagosome membranes as the replication site or hijack the secretion autophagy pathway to promote the maturation and egress of virus particles [18–20]. And inhibition of autophagy contributed to the cellular anti-EV71 effect [21]. Thus, the effect of 6-TG in autophagy upon EV71 infection and the host factor participating in EV71 associated autophagy is investigated in this study.

Here, we found that 6-TG inhibited EV71 replication in vitro. Mechanically, 6-TG inhibited EV71 infection by attenuating the baculoviral IAP repeat containing 3 (BIRC3, also known as cIAP2) mediated complete autophagy. Overall, our study suggests that the BIRC3 antagonist 6-TG may be a plausible candidate for the treatment of EV71-assocaited HFMD.

Methods

Cells, viruses, and compounds

HT-29 (human colorectal cell lines), HeLa (human epithelial carcinoma cell lines) and Vero (African green monkey kidney epithelial cell lines) cells were grown in Dulbecco's modified Eagle's medium (DMEM; HyClone, Logan, UT, USA) supplemented with 10% or 2% fetal bovine serum (FBS; Gibco, Carlsbad, CA, USA) at 37 °C under a 5% CO_2 atmosphere.

EV71-BrCr strain was obtained from Professor Bin Wu, Jiangsu Provincial Centers of Disease Control. EV71 was propagated on Vero cells.

6-Thioguanine (CAS No.154-42-7) was purchased from Selleck Chemicals (Houston, USA), and dissolved in DMSO (final concentration: 40 mM). Ribavirin (CAS No.36791-04-5) and rapamycin (CAS No.53123-88-9) were purchased from MedChem Express (New Jersey, USA), and dissolved in DMSO (final concentration: 10 mM).

siRNAs, plasmids and antibodies

The siBIRC3 targeting BIRC3 (5'-GCCUUGAUGAG AAGUUCCUTT-3') and the negative-control siRNA (siNC) were purchased from RIBOBIO (Guangzhou, China). The plasmid expressing BIRC3 with flag tag (pBIRC3) and the control plasmid (pVector) were purchased from Miaolingbio (Wuhan, China). The plasmids expressing EV71 nonstructural proteins 2A protease ($2A^{pro}$), 2B, 3AB, 3C and 3D were donated by Professor Jianguo Wu from Jinan University. The plasmid expressing EV71 nonstructural protein 2C was prepared by our laboratory [22]. The siRNAs and plasmids were transfected into HeLa cells or HT-29 cells using Lipofectamine 3000 Transfection Kit (Life Technologies, Carlsbad, USA) according to the manufacturer's instructions.

Antibodies used in this study were as follows:

Product name	Company	Product number
Mouse anti-VP1 antibody	Abcam (Cambridge, UK)	ab36367
Mouse anti-β-actin antibody	Santa Cruz Biotechnology (Dallas, USA)	sc-47778
Rabbit anti-LC3 antibody	Sigma-Aldrich (St.Louis, USA)	L7543
Rabbit anti-P62/SQSTM1 antibody	Proteintech (Wuhan, China)	18420-1-AP
Rabbit anti-BIRC3 antibody	ABclonal (Wuhan, China)	A0833
Mouse anti-Flag tag antibody	Servicebio (Wuhan, China)	GB15938-100
Mouse anti-GFP tag antibody	Proteintech (Wuhan, China)	16825-1-AP
Mouse anti-HA tag antibody	Proteintech (Wuhan, China)	66006-1-Ig
Rabbit anti-eIf4G antibody	Cell Signaling Technology (Danvers, USA)	2469
Rabbit anti-GAPDH antibody	Proteintech (Wuhan, China)	10494-1-AP

Cytotoxicity assay

The cytotoxicity of 6-TG or ribavirin was determined by incubating cells with different concentrations of compound for 24 h, and the surviving cells were assayed by CCK8 Cell Counting Kit (Vazyme Biotech, Nanjing, China) as previously described [23]. The 50% cytotoxic concentration (CC_{50}) of 6-TG or ribavirin was calculated based on GraphPad Prism, version 8.0 (GraphPad Software, San Diego, CA, USA).

RNA extraction and quantitative real-time PCR

Total intracellular RNA was extracted using TRIzol reagent (Life Technologies, Carlsbad, USA). Reverse-transcribed cDNA was synthesized using the PrimeScript RT Reagent Kit (TaKaRa, Kyoto, Japan). Quantitative real-time PCR was performed using a standard protocol on an Applied Biosystems 7500 system using SYBR green qPCR Master mix (Vazyme Biotech, Nanjing, China) according to the manufacturer's instruction. GAPDH was used for normalization of mRNA, and analysis was carried out using the $2^{-\Delta\Delta Ct}$ method. The primers used in this study were as follows:

	Forward (5′-3′)	Reverse (5′-3′)
EV71	TAACTGCGGAGCACATACCC	ACGGACACCCAAAGTAGTCG
BIRC3	GCTTTTGCTGTGATGGTGGACTC	CTTGACGGATGAACTCCTGTCC
GAPDH	GAGTCAACGGATTTGGTCGT	CTTGATTTTGGAGGGATCTCGC

Western blot

Cells were collected and lysed using RIPA lysis buffer (Santa Cruz, Dallas, USA). Total protein concentrations were determined using the Bicinchoninic Acid (BCA) Protein Assay Kit (Pierce, Thermo, Massachusetts, USA). Extracted proteins were separated on 10% or 12% SDS-PAGE (BIO-RAD, Hercules, USA) and then transferred onto PVDF membranes (Millipore, Massachusetts, USA). The membranes were blocked for one hour at room temperature and then probed with primary antibodies at an appropriate dilution at 4 °C overnight, followed by incubation with corresponding IRDye 800 goat anti-mouse IgG or IRDye 680 donkey anti-rabbit IgG (LI-COR Bioscience, Lincoln, USA) secondary antibodies. The membranes were scanned by Odyssey Infrared Imaging System (LI-COR Bioscience, Lincoln, USA), and the band intensity of proteins were quantified by ImageJ software.

Virus titers

Vero cells were grown in 96-well plates for 24 h before virus infection. Virus or the collected culture supernatant containing virus was serially diluted in DMEM supplemented with 2% FBS from 10^{-2} to 10^{-8}, and then each diluted sample was added to eight wells in the plate. The plates were then incubated at 37 °C with 5% CO_2. The cytopathic effect (CPE) was recorded under the microscope after 3 days. Virus titers were calculated as the 50% tissue culture infectious dose ($TCID_{50}$) using the Reed–Munch method.

In-cell western assay (ICW assay)

ICW assay was carried out as previously described [24, 25]. Shortly, the cells in 96-well plate were fixed, permeabilized, and blocked with BSA. Then the cells were incubated with EV71 VP1-specific antibody and stained with IRDye 800 goat anti-mouse IgG and nuclear stain DRAQ5 (Thermo, Waltham, USA). Subsequently, the cells were scanned with Odyssey software, and the levels of VP1 protein were quantified and normalized to DRAQ5. The viral inhibition meant the relative levels of VP1 protein and the half-maximal inhibitory concentration (IC_{50}) of 6-TG was calculated using GraphPad Prism as previously described [26].

Time-of-addition assay

HeLa cells were infected with EV71 in 96-wells and then 1 μM 6-TG or DMSO (as a negative control) was added to the cell culture at different time points after virus addition: -2 h, 0 h, 2 h, 4 h, 6 h, 8 h, 12 h and 24 h. At 24 h post infection (hpi), the antiviral activity of 6-TG was determined by ICW assay.

Immunofluorescence assay

Immunofluorescence assay was carried out as previously described [27]. In short, the cells were fixed by 4% paraformaldehyde (Servicebio, Wuhan, China), permeabilized by 0.5% Triton X-100, and followed by blocking with 2% BSA. Then the cells were incubated with primary antibodies at 4 °C for 12 h. Subsequently, the cells were

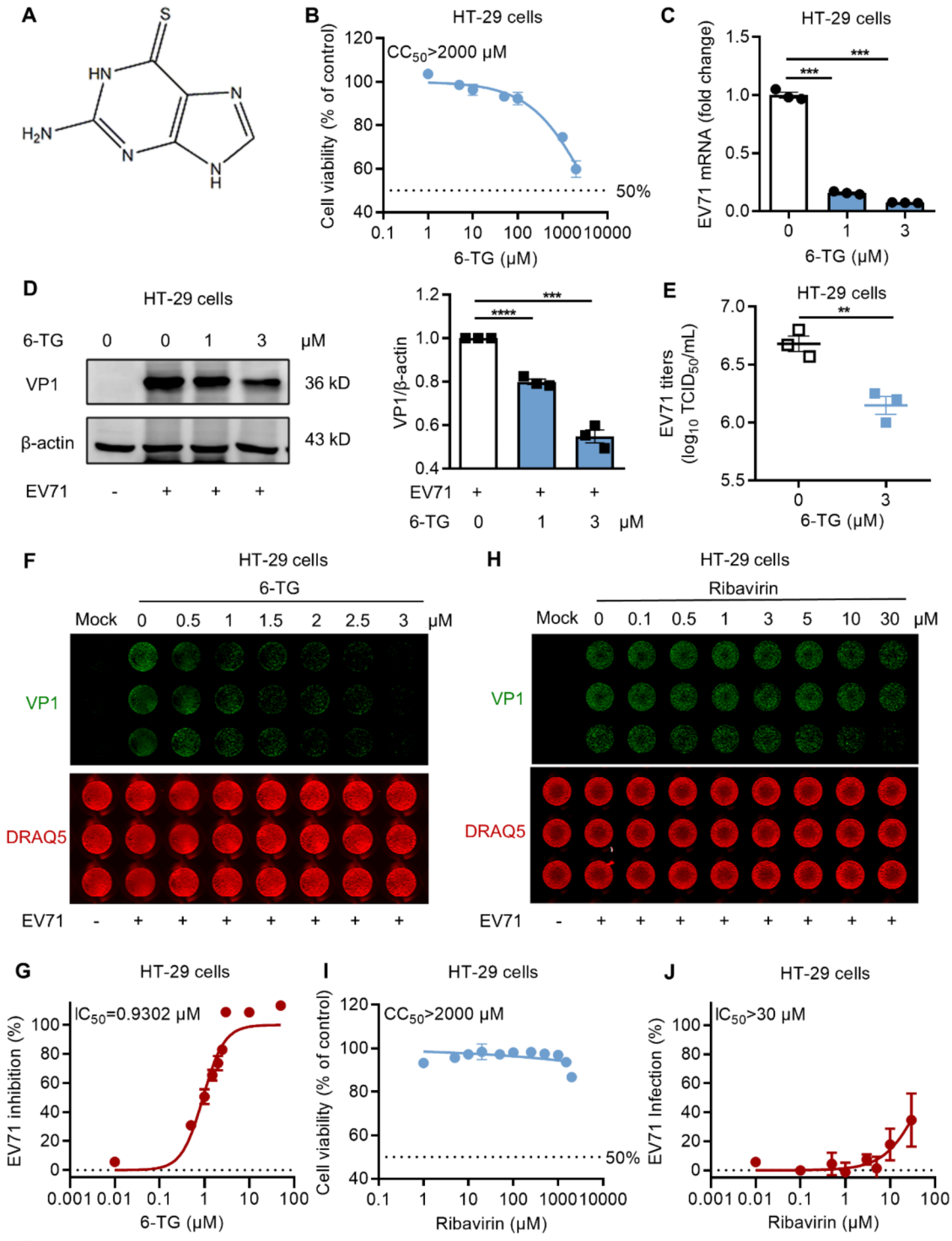

K

Compounds	IC_{50} (μM)	CC_{50}(μM)	SI (CC_{50}/IC_{50})
6-TG	0.9302	>2000	>2150.1
Ribavirin	>30	>2000	>66.7

Fig. 1 (See legend on next page.)

(See figure on previous page.)

Fig. 1 6-TG inhibited EV71 infection. (**A**) The molecular structure of 6-TG was shown. (**B**) HT-29 cells were treated with serial concentrations (0-2000 μM) of 6-TG for 24 h, then the cell viability of the cells was determined by CCK8 assay. The viability of non-treated cells was considered as a blank control. The 6-TG-treated cell viability was determined as a percentage of the blank control. CC_{50} is 50% cytotoxicity concentration of 6-TG in HT-29 cells. (**C**) HT-29 cells were infected with EV71 at an MOI of 3 in the presence of 6-TG (0, 1, 3 μM). After 24 h, EV71 mRNA was quantified via quantitative real-time PCR, normalized against GAPDH. The EV71 VP1 protein expression was quantified via western blot analysis, normalized against β-actin. The intensity of western blot bands signals was quantified by ImageJ software (**D**). (**E**) HT-29 cells were infected with EV71 at an MOI of 3 for 4 h, then the cells were washed with PBS and incubated with 3 μM 6-TG. After 24 h, the culture supernatant was collected and added to Vero cells, the viral titers were calculated as the $TCID_{50}$ after 72 h incubation. (**F**) HT-29 cells were infected with EV71 at an MOI of 3 in the presence of 6-TG at different concentrations (0, 0.5, 1, 1.5, 2, 2.5, 3 μM). After 24 h, the intracellular EV71 VP1 (green) was examined via ICW assay and normalized by DRAQ5 (red). (**G**) HT-29 cells were infected with EV71 at an MOI of 3 in the presence of 6-TG at different concentrations (0, 0.5, 1, 1.5, 2, 2.5, 3, 10, 50 μM). After 24 h, the intracellular EV71 VP1 was examined via ICW assay and normalized by DRAQ5. The percent of EV71 inhibition was analyzed by Odyssey software. The intracellular EV71 VP1 of EV71-infected cells without 6-TG-treatment was considered as a negative control. IC_{50} is 50% inhibitory concentration of 6-TG against EV71. (**H**) HT-29 cells were infected with EV71 at an MOI of 3 in the presence of ribavirin at different concentrations (0, 0.1, 0.5, 1, 3, 5, 10, 30 μM). After 24 h, the intracellular EV71 VP1 (green) was examined via ICW assay and normalized by DRAQ5 (red). The percent of EV71 inhibition was analyzed by Odyssey software, and the intracellular EV71 VP1 of EV71-infected cells without ribavirin treatment were considered as a negative control. IC_{50} is 50% inhibitory concentration of ribavirin against EV71 (**J**). (**I**) HT-29 cells were treated with serial concentrations (0-2000 μM) of ribavirin for 24 h, then cell viability of the cells was determined by CCK8 assay. The viability of non-treated cells was considered as a blank control. The ribavirin-treated cell viability was determined as a percentage of the blank control. (**K**) The IC_{50}, CC_{50}, and SI index of 6-TG or ribavirin against EV71 in HT-29 cells. SI is selectivity index of compounds, and was defined as the ratio of CC_{50} to IC_{50} (CC_{50}/IC_{50}). Data were pooled from four (**B** and **I**) or three (**C**, **D**, **E**, **G** and **J**) independent experiments, and were shown as the mean ± SEM (**$P < 0.01$, ***$P < 0.001$, ****$P < 0.0001$)

incubated with Alexa Fluro 594-labeled donkey anti-rabbit IgG or Alexa Fluro 488-labeled goat anti-mouse IgG (Thermo, Waltham, USA) for about 1 h, and the cell nucleus were stained by DAPI. The cells were examined under and imaged by Olympus Fluoview FV3000 as previously described [28].

Statistical analysis

The data was expressed as the mean ± standard error of the mean (SEM) of three independent experiments. The levels of significance for the different experimental groups were analyzed using *Student t*-tests and *one-way* ANOVA followed by a *SNK-q* test. *P*-value < 0.05 was considered statistically significant (ns, no significant, *$P < 0.05$, **$P < 0.01$, ***$P < 0.001$, and ****$P < 0.0001$).

Results

6-TG inhibits EV71 infection

6-TG, also named 2-Amino-6-purinethiol, is a synthetic guanosine analog with the molecular structure as shown in Fig. 1A. To determine the cytotoxic effects of 6-TG, HT-29 cells were treated with 6-TG at increasing concentrations from 1 to 2000 μM for 24 h. The 50% cytotoxicity concentration of 6-TG (CC_{50}) to HT-29 cells was greater than 2000 μM (Fig. 1B). Subsequently, EV71-infected HT-29 cells were treated with 6-TG from 0 to 3 μM, and we observed that 6-TG significantly reduced EV71 mRNA levels (Fig. 1C). Furthermore, VP1 protein of EV71, the major contributor to EV71 pathogenesis [29, 30], was significantly decreased in the presence of 6-TG at 1 or 3 μM, respectively (Fig. 1D). As expected, 6-TG also significantly reduced the extracellular EV71 titers as compared to the untreated group (Fig. 1E). Taken together, these results indicated that 6-TG effectively suppressed EV71 replication and proliferation in vitro.

Next, the 50% inhibitory concentration (IC_{50}) of 6-TG against EV71 was determined by ICW assay in HT-29 cells, and EV71 VP1 protein was significantly reduced at an IC_{50} of 0.9302 μM (Fig. 1F-G), which was significantly lower than the cytotoxic concentration. Ribavirin was previously reported to exhibit an anti-EV71 activity [31], therefore, ribavirin was used as a positive control to assess the anti-EV71 activity of 6-TG in this study. The IC_{50} of ribavirin was over 30 μM with the $CC_{50} > 2000$ μM (Fig. 1H-J). The selectivity index (SI, CC_{50}/IC_{50}) of 6-TG was > 2150.1, higher than ribavirin (> 66.7) (Fig. 1K), suggesting that 6-TG is a more potent drug for inhibiting EV71 than ribavirin.

6-TG inhibits EV71 replication at early stages of viral infection

HeLa cells were widely used to explore the antiviral effects of 6-TG or the EV71 replication process [14, 15, 27]. We found that 6-TG at 1 μM, much lower than CC_{50} at 22.42 μM, showed 88% inhibitory effect of EV71 (Fig. 2A-B). To determine at which stage of EV71 replication the anti-EV71 activity of 6-TG occurred, time-of-addition experiment was further performed in HeLa cells. 1 μM 6-TG was added to HeLa cells at different time points (-2, 0, 2, 4, 6, 8, 12 and 24 h) during infection, and the EV71 VP1 expression relative to the DMSO-treated cells was measured using ICW assay at 24 hpi (hours post EV71 infection) (Fig. 2C). At present, 6-TG inhibited almost 100% of EV71 VP1 protein at -2 hpi, > 90% at 2 hpi, and close to 50% at 12 hpi (Fig. 2D-E). These data indicated that 6-TG likely acted on the early stages of EV71 infection.

BIRC3 is a key factor for 6-TG inhibiting EV71 replication

Previous studies have considered Ras-related C3 botulinum toxin substrate 1 (Rac1) to be one of the main

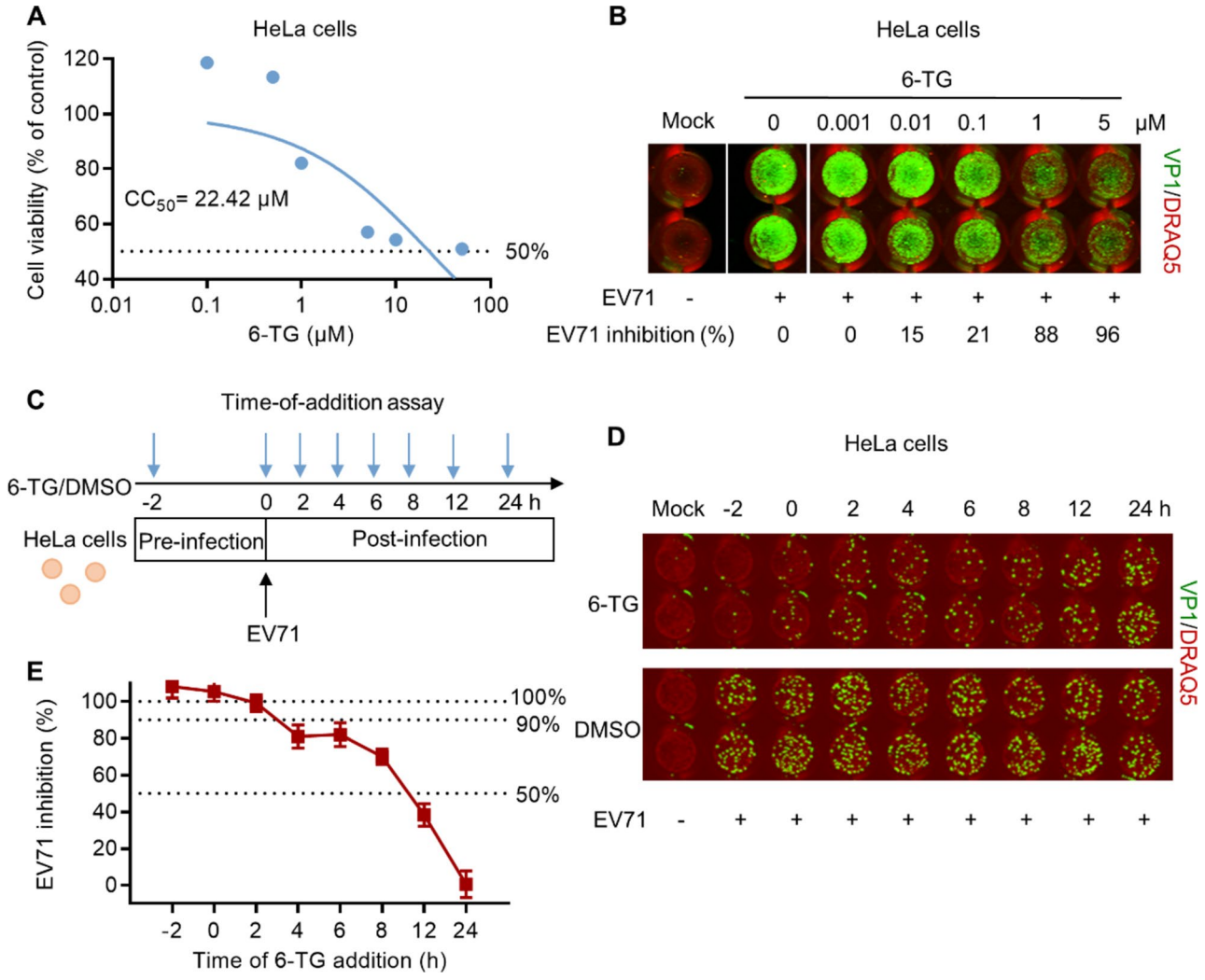

Fig. 2 6-TG inhibited EV71 replication at early stages of viral infection. (**A**) HeLa cells were treated with serial concentrations (0–50 μM) of 6-TG for 24 h, then the cell viability of the cells was determined by CCK8 assay. The viability of non-treated cells was considered as a blank control. The 6-TG-treated cell viability was determined as a percentage of the blank control. CC_{50} is 50% cytotoxicity concentration of 6-TG in HeLa cells. (**B**) HeLa cells were infected with EV71 at an MOI of 1 in the presence of 6-TG at different concentrations (0, 0.001, 0.01, 0.1, 1, 5 μM). After 24 h, the intracellular EV71 VP1 (green) was examined via ICW assay and normalized by DRAQ5 (red). The percent of EV71 inhibition was analyzed by Odyssey software, and the intracellular EV71 VP1 of EV71-infected cells without 6-TG treatment were considered as a negative control. (**C**) The design of action mode of time-of-addition assay. HeLa cells were infected with EV71 (MOI = 0.5) for 24 h, and 1 μM of 6-TG or DMSO were added to cells at -2, 0, 2, 4, 6, 8, 12 and 24 h of EV71 infection. After 24 h, the intracellular EV71 VP1 (green) was examined via ICW assay (**D**). The percent of inhibition of EV71 was analyzed by Odyssey software, and the intracellular EV71 VP1 of EV71-infected cells with DMSO-treatment was considered as control (**E**). –2 –0 h: viral pre-infection period; 0–2 h: viral adsorption and entry period; 2–24 h: the period of virus proliferation in the cells. 6-TG inhibited almost 100% of EV71 VP1 protein at -2 hpi, > 90% at 2 hpi, and close to 50% at 12 hpi. Data were pooled from four (**A**) or three (**E**) independent experiments, and were shown as the mean ± SEM

targets of 6-TG [32], and we previously found that 6-TG inhibited SFTSV and HSV-1 replication via suppressing the expression and/or activity of Rac1 [14, 15]. Therefore, we initially investigated the role of Rac1 in 6-TG-induced EV71 inhibition, and found that NSC23766, a Rac1-specific inhibitor, had no effect on EV71 infection (Fig. 3A), which implies that the mechanism by which 6-TG inhibits its EV71 replication is distinct from that of SFTSV or HSV-1. Subsequently, we reanalyzed two related RNA-sequencing datasets: one reported in our previous study (Control vs. 6-TG without viral infection) [15], and the other available in the GEO database (Mock vs. EV71 without 6-TG treatment, GSE:123550). We identified 14 genes appeared to overlap between the two datasets (Fig. 3B), and the BIRC3 was downregulated by 6-TG treatment and upregulated by EV71 infection, implying that BIRC3 might play a key role in 6-TG against EV71 infection (Fig. 3C). Here, both mRNA and protein levels of BIRC3 were decreased in 6-TG treated HeLa cells and HT-29 cells (Fig. 3D-E and Fig. S1A-B), indicating that BIRC3 might be another target of 6-TG. Moreover, EV71 infection elevated both the mRNA and protein levels of

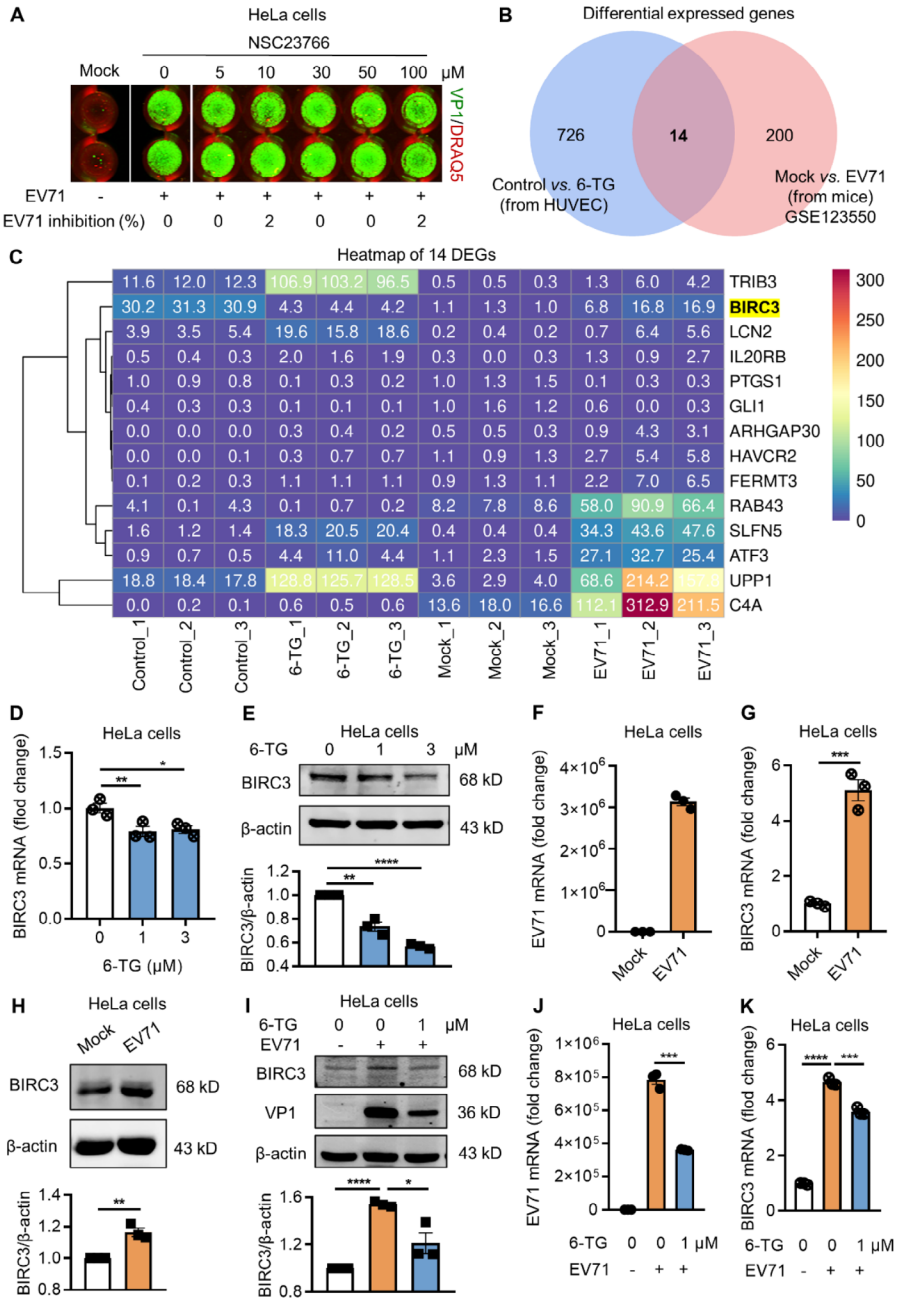

Fig. 3 BIRC3 was the key regulator of 6-TG against EV71 infection. (**A**) HeLa cells were infected with EV71 at an MOI of 1 in the presence of NSC23766 at different concentrations (0, 5, 10, 30, 50, 100 μM). After 24 h, the intracellular EV71 VP1 (green) was examined via ICW assay and normalized by DRAQ5 (red). The percent of EV71 inhibition was analyzed by Odyssey software, and the intracellular EV71 VP1 of EV71-infected cells without NSC23766 treatment were considered as a negative control. (**B**) Identification of 14 common differential expressed genes (DEG) from untreated or 6-TG-treated HUVEC database (Control vs. 6-TG) and uninfected or EV71-infected mice database (GSE123550) (Mock vs. EV71) through SangerBox 3.0 online tools. Advanced Pie plot was performed using the OmicStudio tools at https://www.omicstudio.cn/tool. (**C**) The heatmap of the 14 common DEGs from Control vs. 6-TG group and Mock vs. EV71 group. Advanced Heatmap Plots was performed using the OmicStudio tools at https://www.omicstudio.cn. (**D** and **E**) HeLa cells were incubated with 1 or 3 μM 6-TG for 2 h. Then the BIRC3 mRNA was quantified by quantitative real-time PCR, normalized to GAPDH (**D**). The BIRC3 protein levels were quantified via western blot analysis, normalized against β-actin. The intensity of western blot bands signals was quantified by ImageJ software (**E**). (**F**, **G** and **H**) HeLa cells were infected with EV71 at an MOI of 0.5 for 24 h, and the EV71 mRNA and BIRC3 mRNA was quantified via quantitative real-time PCR, normalized against GAPDH (**F** and **G**). The BIRC3 expression was quantified via western blot analysis, normalized against β-actin. The intensity of western blot bands signals was quantified by ImageJ software (**H**). (**I**, **J** and **K**) HeLa cells were infected with EV71 at an MOI of 0.5 in the presence of 6-TG at 1 μM. The BIRC3 and EV71 VP1 expression was quantified via western blot analysis, normalized against β-actin. The intensity of BIRC3 was quantified by ImageJ software (**I**). The EV71 mRNA and BIRC3 mRNA was quantified via quantitative real-time PCR, normalized against GAPDH (**J** and **K**). Data were pooled from three (**D**-**K**) independent experiments, and were shown as the mean ± SEM (*$P < 0.05$, **$P < 0.01$, ***$P < 0.001$, ****$P < 0.0001$)

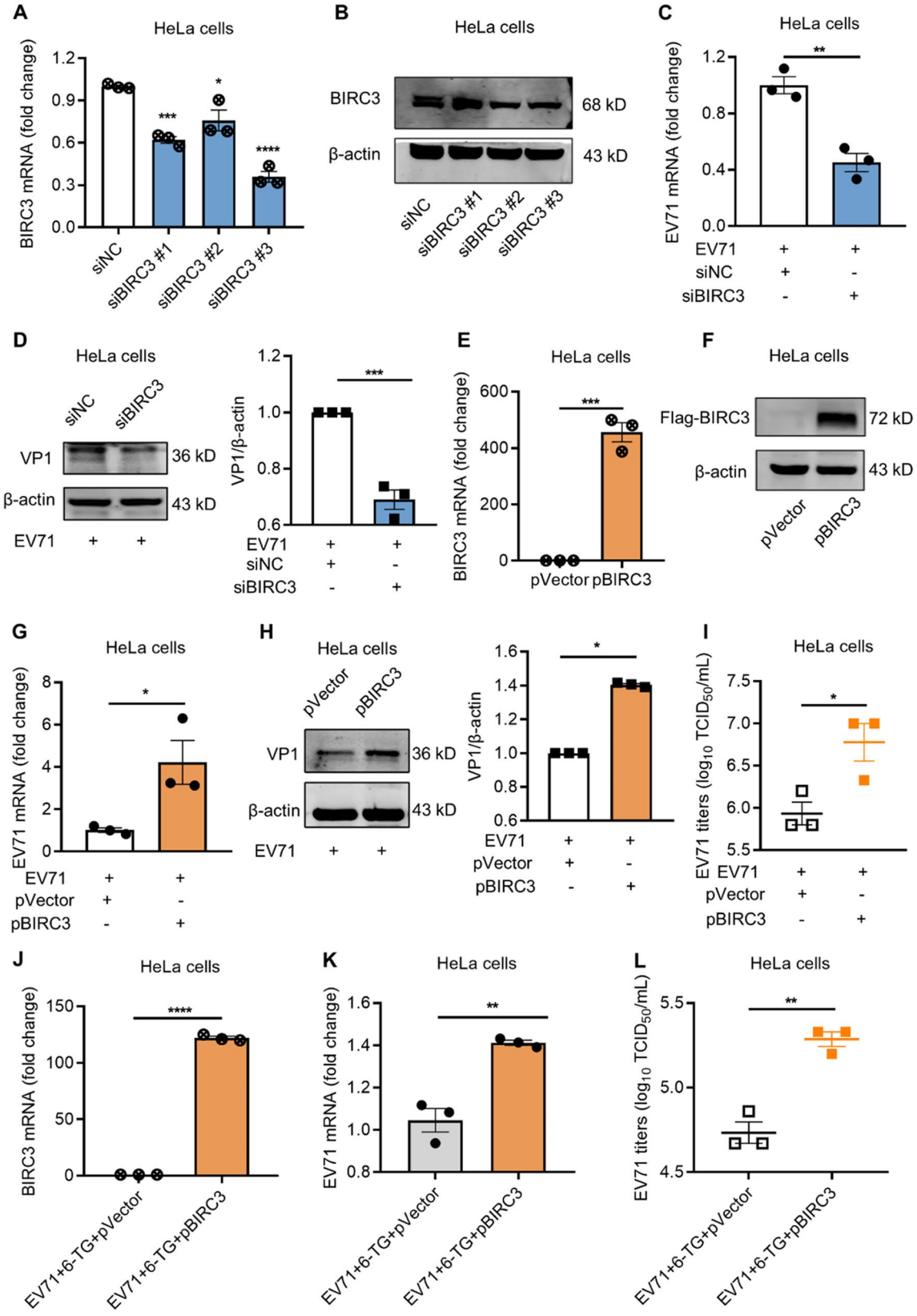

Fig. 4 (See legend on next page.)

(See figure on previous page.)

Fig. 4 BIRC3 promoted EV71 replication and reversed the anti-EV71 effect of 6-TG. (**A** and **B**) HeLa cells were transfected with three specific siRNAs targeting BIRC3 (siBIRC3 #1, siBIRC3 #2, siBIRC3 #3) or control siRNA (siNC) for 30 h. The cells were harvested and the BIRC3 RNA levels were quantified via quantitative real-time PCR, normalized against GAPDH (**A**), the BIRC3 protein levels were evaluated by western blot assay, normalized to β-actin (**B**). (**C** and **D**) HeLa cells were transfected with siBIRC3 or siNC for 30 h, and then infected with EV71 at an MOI of 0.5 for 24 h. The cells were harvested and the EV71 RNA levels were quantified via quantitative real-time PCR, normalized against GAPDH (**C**). The EV71 VP1 protein expression was evaluated by western blot assay, normalized to β-actin. The intensity of western blot bands signals was quantified by ImageJ software (**D**). (**E** and **F**) HeLa cells were transfected with 1 μg plasmid encoding BIRC3 (pBIRC3) or control plasmid (pVector). After 30 h, the cells were collected, and the BIRC3 RNA levels were quantified via quantitative real-time PCR, normalized against GAPDH (**E**), the flag-BIRC3 protein expression was evaluated by western blot assay, normalized to β-actin (**F**). (**G** and **H**) HeLa cells were transfected with 1 μg pBIRC3 or pVector for 30 h, and then infected with EV71 at an MOI of 0.5 for 24 h. The cells were harvested and EV71 RNA levels were quantified via quantitative real-time PCR, normalized against GAPDH (**G**). The EV71 VP1 protein expression in harvested cells was evaluated by western blot assay, normalized to β-actin. The intensity of western blot bands signals was quantified by ImageJ software (**H**). (**I**) HeLa cells were transfected with 1 μg pBIRC3 or pVector for 30 h, and next infected with EV71 at an MOI of 0.5 for 2 h, then the cells were washed with PBS and incubated with clear culture medium. After 24 h, the culture supernatant was collected and added to Vero cells, the viral titers were calculated as the $TCID_{50}$ after 72 h incubation. (**J** and **K**) HeLa cells were transfected with 1 μg pBIRC3 or an empty Vector for 30 h, then the cells were infected with EV71 at an MOI of 0.5 in the presence of 1 μM 6-TG for 24 h. The EV71 RNA levels and the BIRC3 RNA levels in harvested cells were quantified via quantitative real-time PCR, normalized against GAPDH. (**L**) HeLa cells were transfected with 1 μg pBIRC3 or an empty Vector for 30 h, then the cells were infected with EV71 at an MOI of 0.5 for 2 h. After washing with PBS, the cells were incubated with 1 μM 6-TG for 24 h. The culture supernatant was collected and added to Vero cells, the viral titers were calculated as the $TCID_{50}$ after 72 h incubation. Data were pooled from three (**A**, **C-E** and **G-L**) or two (**B** and **F**) independent experiments, and were shown as the mean ± SEM (*$P < 0.05$, **$P < 0.01$, ***$P < 0.001$, ****$P < 0.0001$)

BIRC3 in HeLa cells and HT-29 cells (Fig. 3F-H and Fig. S1C-E), indicating that BIRC3 may be involved in EV71 infection. Importantly, the inhibition of EV71 replication by 6-TG treatment was accompanied by a decrease in BIRC3 (Fig. 3I-K). Overall, these results suggested that BIRC3 might be a key factor for 6-TG suppressing EV71 replication.

6-TG exhibits anti-EV71 effect by downregulating BIRC3

Next, we analyzed the roles of BIRC3 in EV71 replication. BIRC3 was silenced by siBIRC3 #1/2/3 as measured in both mRNA expression (Fig. 4A) and protein levels (Fig. 4B), and siBIRC3 #3 (called siBIRC3 in the following text) exhibited the most pronounced inhibition of BIRC3. Silencing BIRC3 markedly reduced EV71 mRNA (Fig. 4C) and VP1 protein (Fig. 4D) as compared to siNC-transfected HeLa cells. Furthermore, the plasmid expressing BIRC3 (pBIRC3) was also confirmed in both mRNA (Fig. 4E) and protein levels (Fig. 4F), and the overexpressed BIRC3 resulted in increased EV71 mRNA levels, VP1 protein levels and viral titers (Fig. 4G-I) as compared to an empty vector-transfected HeLa cells. Although we failed to knock down BIRC3 in HT-29 cells, we also observed a positive effect of BIRC3 overexpression in HT-29 cells on EV71 replication (Fig. S2A-C). Importantly, we found that BIRC3 overexpression reversed the inhibitory effect of 6-TG on EV71 replication and production (Fig. 4J-L). These results suggested that BIRC3 was required for EV71 replication in vitro, and the anti-EV71 effect of 6-TG was depend on BIRC3.

BIRC3 is necessary for the cleavage function of EV71 $2A^{pro}$ and the expression of EV71 3AB

The nonstructural proteins $2A^{pro}$–2C and 3A–3D of EV71 are involved in regulating viral replication [33], and $2A^{pro}$ exhibits the cysteine protease activity in cleaving the polyprotein into mature proteins of EV71 and cleaving the elongation factor eIF4G to inhibit host cap-dependent protein synthesis. Therefore, previous studies usually used the cleaved eIF4G/β-actin to present the cleavage function of $2A^{pro}$ [34, 35]. Then we investigated the effect of BIRC3 on nonstructural protein function or expression by transfecting plasmids GFP-$2A^{pro}$/2B/3AB/3C/3D and HA-2C in HeLa cells for 24 h followed by siNC or siBIRC3 treatment for 30 h. The results showed that the function of $2A^{pro}$ to cleavage eIF4G and the expression of 3AB were significantly reduced upon BIRC3 knocking down (Fig. 5). Altogether, these results suggested that BIRC3 might be an important regulator on the cleavage function of EV71 $2A^{pro}$ and the expression of EV71 3AB.

6-TG results in EV71 inhibition by attenuating BIRC3-mediated complete autophagy

Recently, the role of BIRC3 in Crohn's disease, one disease of IBD, in relation to autophagy has attracted our interests [36], due to autophagy supports EV71 replication [19]. The complete autophagy ranges from the autophagosome formation, the autophagosome-lysosome fusion and lysosome-mediated cargoes degradation [37]. Firstly, we observed that the autophagosome marker GFP-LC3 puncta was formed at 12 hpi in EV71-infected HeLa cells (Fig. 6A), as well as the ratio of LC3 II to LC3 I and the degradation of autophagy cargo receptor P62/SQSTM1 (sequestosome 1) was also increased at 12 and 24 hpi in HeLa cells (Fig. 6B), which indicated that EV71 infection induced the complete autophagy. Secondly, we investigated the role of 6-TG in EV71-induced complete autophagy, and observed that 6-TG caused an increase of LC3 II/LC3 I ratio and P62 levels in HeLa cells, which was associated with EV71 inhibition (Fig. 6C). It meant a large number of autophagosomes carrying P62-linked cargoes were stranded, and the complete autophagy was affected. We also found the increased P62 levels and

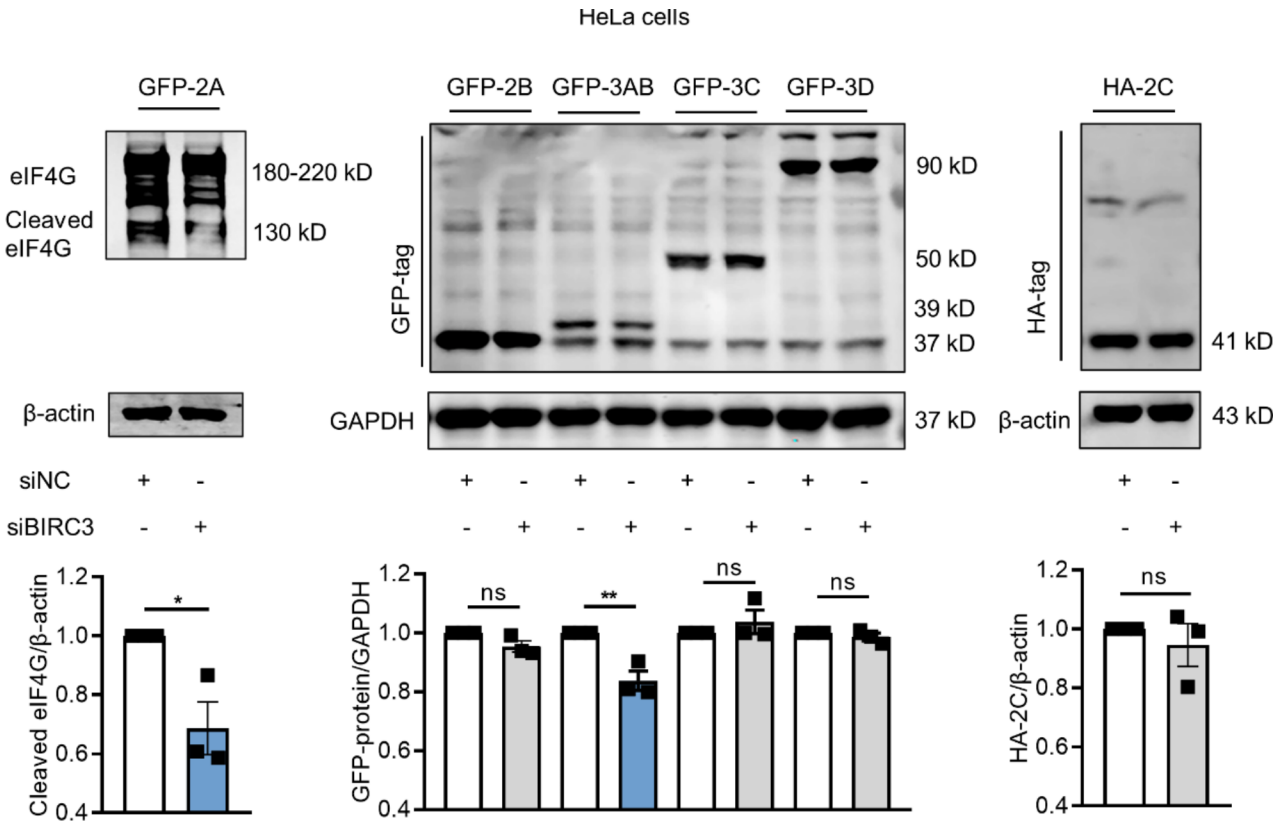

Fig. 5 BIRC3 knockdown affected the cleavage function of EV71 2A^{pro} and the expression of EV71 3AB. HeLa cells were transfected with plasmid GFP-2A^{pro}, GFP-2B, GFP-3AB, GFP-3C, GFP-3D and HA-2C for 24 h, then were transfected with siBIRC3 or siNC for 30 h. The cells were harvested and the expression of eIF4G, GFP-tag, HA-tag was evaluated by western blot assay, normalized to β-actin or GAPDH. The intensity of western blot bands signals of cleaved eIF4G, GFP-2B/3AB/3 C/3D, HA-2 C, β-actin and GAPDH were quantified by ImageJ software. Data were pooled from three independent experiments, and were shown as the mean ± SEM (ns, no significant, *$P < 0.05$, **$P < 0.01$)

decreased EV71 VP1 levels in 6-TG-treated HT-29 cells (Fig. S3). Furthermore, we found the elevated LC3 II/LC3 I ratio in BIRC3-knockdown HeLa cells, accompanying by a decrease in EV71 VP1 expression (Fig. 6D). Overall, these results suggested that the accumulated autophagosomes induced by 6-TG treatment and BIRC3 shortage damaged EV71 infection.

Next, we treated HeLa cells with 6-TG treatment alone, and the results showed that 6-TG at 1 or 3 μM increased the LC3 II/LC3 I ratio as well as the P62 levels (Fig. 7A). Moreover, we added 1 μM 6-TG to 100 nM rapamycin (an autophagy activator, inhibits mTOR activity)-pretreated HeLa cells, and also found an increased LC3 II/LC3 I ratio and increased P62 expression following 6-TG treatment (Fig. 7B). We further investigated the relationship between BIRC3 and autophagy in HeLa cells without infection. We found that the LC3 II/LC3 I ratio was increased in BIRC3 overexpressed HeLa cells, the P62 levels was not affected (Fig. 7C). And both the LC3 II/LC3 I ratio and the P62 expression were increased in BIRC3 knockdown HeLa cells (Fig. 7D), which was the same effect as 6-TG treatment on autophagosome accumulation and complete autophagy blockage. These results indicated that 6-TG blocked BIRC3-mediated complete autophagy.

Discussion

In this study, we have demonstrated that 6-TG exhibited an activity against EV71 infection. And 6-TG exhibited more potent inhibitory activity against EV71 than ribavirin, requiring less than 1/30 molar concentration of ribavirin to reach IC_{50}. 6-TG could completely inhibit EV71 replication at about 3 μM in vitro, which was in contrast to ribavirin that failed to completely inhibit or abrogate clinical manifestation of EV71 [38].

EV71 has developed strategies to hijack the complete autophagy including autophagosome production, autophagosome fusion with lysosomes and followed degradation to help viral replication and maturation [20, 39]. In this study, we found that 6-TG addition with or without EV71 infection increased cellular LC3 II/LC3 I ratio and autophagy cargo receptor P62 levels, and this accumulated autophagosomes and blocked complete autophagy flux damaged EV71 infection. Previous studies reported that knocking down the proteins involved in the fusion between autophagosomes and lysosomes, such as

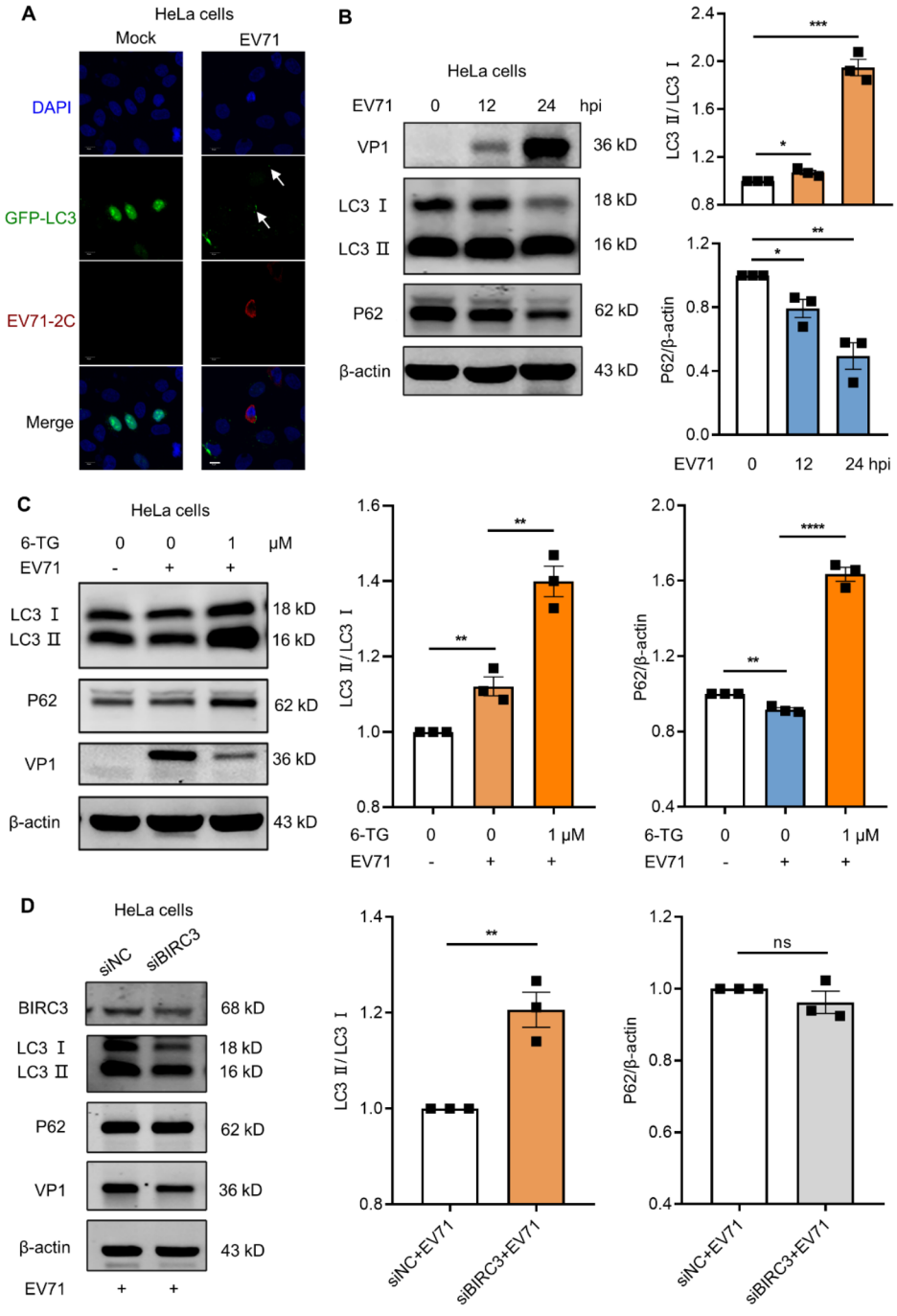

Fig. 6 6-TG suppressed EV71 replication by diminishing BIRC3-mediated autophagy. (**A**) HeLa cells were Mock-infected or EV71 (MOI = 0.5) infected for 12 h, then cells were fixed for immunostaining using EV71 2C antibody (red). Nuclei were labeled with DAPI (blue). Scale bars, 10 μm. The white arrows showed the formed GFP-LC3 puncta. (**B**) HeLa cells were infected with EV71 at an MOI of 0.5, and the cells were harvested at 12, 24 hpi (hours post infection). The EV71 VP1, LC3 I, LC3 II and P62 expression was quantified via western blot analysis, normalized against β-actin. The intensity of western blot bands signals of LC3 II/LC3 I and P62/β-actin was quantified by ImageJ software. (**C**) HeLa cells were infected with EV71 at an MOI of 0.5 in the presence of 1 μM 6-TG. After 24 h, the EV71 VP1, LC3 I, LC3 II and P62 expression was quantified via western blot analysis, normalized against β-actin. The intensity of western blot bands signals of LC3 II/LC3 I and P62/β-actin was quantified by ImageJ software. (**D**) HeLa cells were transfected with siBIRC3 or siNC for 30 h, then the cells were infected with EV71 at an MOI of 0.5 for 24 h. The BIRC3, LC3 I, LC3 II, P62 and EV71 VP1 expression in harvested cells was quantified via western blot analysis, normalized against β-actin. The intensity of western blot bands signals of LC3 II/LC3 I and P62/β-actin was quantified by ImageJ software. Data were pooled from three (**B-D**) or two (**A**) independent experiments, and were shown as the mean ± SEM (ns, no significant, *$P < 0.05$, **$P < 0.01$, ***$P < 0.001$, ****$P < 0.0001$)

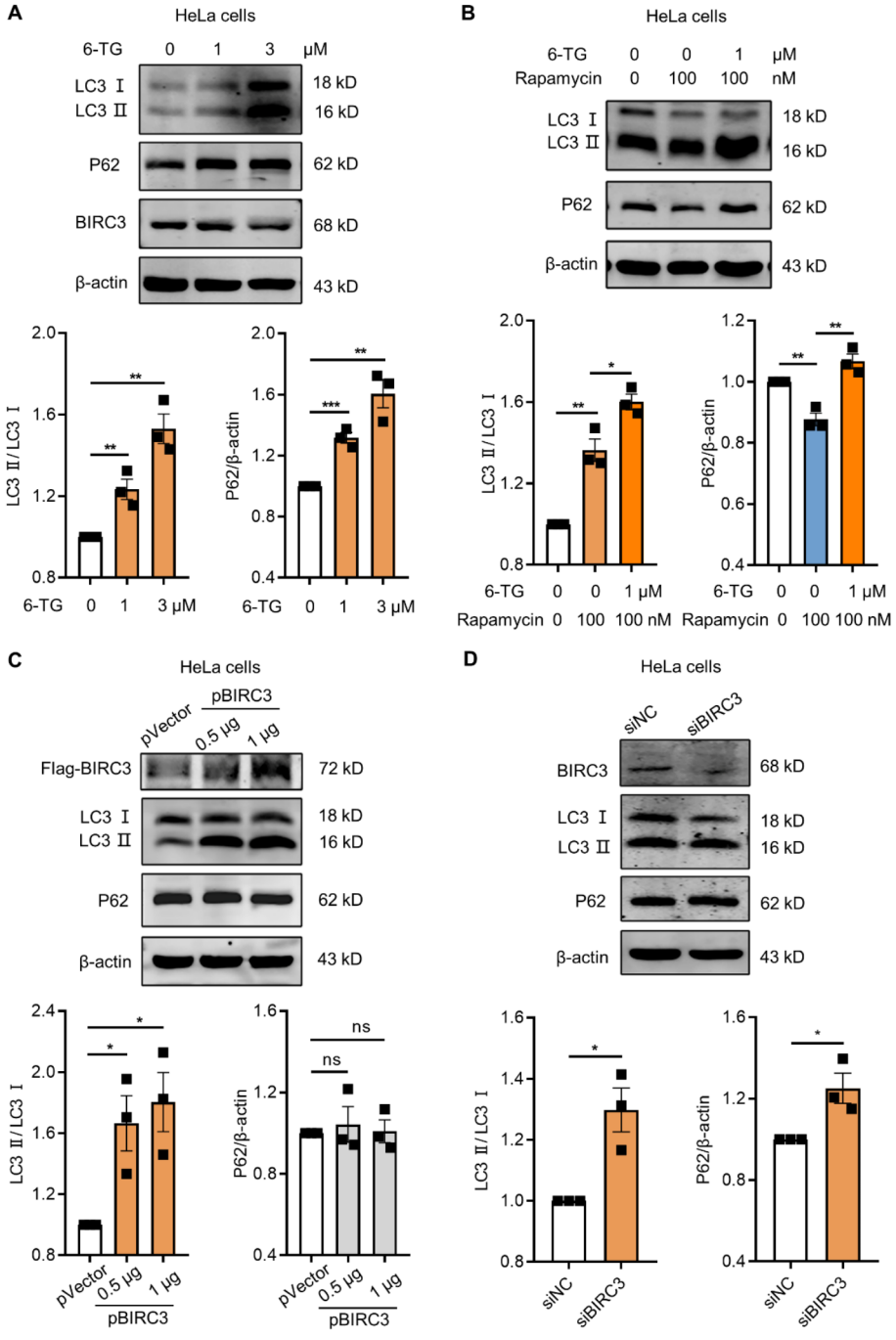

Fig. 7 6-TG addition diminished BIRC3-mediated autophagy. (**A**) HeLa cells were incubated with 1 or 3 μM 6-TG for 24 h, the LC3 I, LC3 II, P62 and BIRC3 expression was quantified via western blot analysis, normalized against β-actin. The intensity of western blot bands signals of LC3 II/LC3 I and P62/β-actin was quantified by ImageJ software. (**B**) HeLa cells were stimulated with 100 nM rapamycin for 12 h, then they were incubated with 1 μM 6-TG for 24 h. The LC3 I, LC3 II and P62 expression was quantified via western blot analysis, normalized against β-actin. The intensity of western blot bands signals of LC3 II/LC3 I and P62/β-actin was quantified by ImageJ software. (**C**) HeLa cells were transfected with 0.5–1 μg pBIRC3 or pVector for 30 h. The cells were harvested and Fag-BIRC3, LC3 I, LC3 II and P62 expression was evaluated by western blot assay, normalized to β-actin. The intensity of western blot bands signals of LC3 II/LC3 I and P62/β-actin was quantified by ImageJ software. (**D**) HeLa cells were transfected with siBIRC3 or siNC for 30 h, respectively. The cells were harvested and BIRC3, LC3 I, LC3 II and P62 expression was evaluated by western blot assay, normalized to β-actin. The intensity of western blot bands signals of LC3 II/LC3 I and P62/β-actin was quantified by ImageJ software. Data were pooled from three (**A**-**D**) independent experiments, and were shown as the mean ± SEM (ns, no significant, *$P < 0.05$, **$P < 0.01$, ***$P < 0.001$)

STX17 and SNAP29, or blocking autolysosomal acidification by knocking down the associated protein ATP6AP2, inhibited EV71 infection [40, 41]. In our study, we found that knocking down BIRC3, the anti-EV71 target of 6-TG explored here, significantly reduced EV71 replication by inducing autophagosome accumulation and complete autophagy blockage. Since BIRC3 was required for effective fusion of autophagosomes with lysosomes [36], the failure of autophagosome and lysosome fusion and blocked complete autophagy due to the lack of BIRC3 may mediate the antiviral effect of 6-TG. We also found that overexpression of BIRC3 promoted the increased LC3 II/LC3 I ratio but no change in P62, suggesting that the role of BIRC3 on promoting the fusion of autophagosomes with lysosomes may not be effective in the absence of viral infection due to the over-activated autophagy is harmful to maintain cellular homeostasis [42].

However, the mechanism of 6-TG regulation of BIRC3 expression has not been fully elucidated in our study. 6-TG was reported to down-regulate DNA methyltransferase 1 (DNMT1)-mediated DNA methylation to activate apoptosis-modulating protein (DAXX) [43], and activated DAXX acted as a transcriptional repressor repressing transcription factor NF-κB member (RelB), resulting in decreased mRNA levels of targeted gene BIRC3 [44]. Thus, the decrease in BIRC3 mRNA levels after 6-TG treatment may be related to reduced DNMT1. 6-TG has also been reported to facilitate the proteasome-mediated degradation of DNMT1 in leukemic cells [45], thus, the role of the ubiquitin proteasome system in the 6-TG-induced reduction of BIRC3 protein could be a possible mechanism.

Enterovirus including EV71 usually use autophagosome maturation to serve as the site of genome replication, and several membrane-associated viral proteins interact with the replication organelle [46]. Inhibition of acidification of the autophagy-induced membranous compartment not only suppressed viral infection, but also destabilized viral proteins, which may be due to the altered protein association with membranes and then leading to their degradation in the cytoplasm [47]. In our study, we found that BIRC3 knockdown declined the cleavage function of EV71 $2A^{pro}$ and expression of EV71 3AB. EV71 $2A^{pro}$ is a cysteine protease responsible for cleaving of the open reading frame of EV71 (which can be categorized into three regions, P1, P2 and P3) into the P1 and P2 precursor polyproteins. EV71 3AB, derived from the P3 precursor polyproteins of EV71, contains N-terminal 3A and C-terminal 3B/VPg domains and will be proteolytically cleaved into proteins 3A and 3B/VPg. 3A, 3B/VPg as well as 3AB play critical roles in EV71 RNA synthesis, and 3A has an effect on protein trafficking while 3B/VPg functions as a primer to initiate RNA synthesis by EV71 3D [48]. EV71 3A also reported to increase viral replication and growth by upregulating autophagy degradation-related protein LRRC25 [49, 50]. Thus, BIRC3 knockdown resulted in the accumulated autophagosomes and autophagy cargoes-linked P62 may not provide the acidified replication environments to destabilize EV71 $2A^{pro}$ and 3AB, resulting EV71 inhibition.

Conclusions

Our present work demonstrated that 6-TG had a significant antiviral activity against EV71, and the antiviral activity was likely based on suppressing the host protein BIRC3-mediated the complete autophagy. And due to its good in vitro safety profile and high SI value than ribavirin, 6-TG is a potential therapeutic candidate for the further study for EV71-induced HFMD.

Abbreviations

6-TG	6-thioguanine
EV71	Enterovirus 71
BIRC3	Baculoviral IAP repeat containing 3
HFMD	Hand, foot, and mouth disease
CC_{50}	50% cytotoxicity concentration of compounds
IC_{50}	50% inhibitory concentration of compounds against virus
SI	Selectivity index
FDA	US Food and Drug Administration
IBD	Inflammatory bowel disease
SARS-COV-2	Severe acute respiratory syndrome coronavirus 2
SFTSV	Severe fever with thrombocytopenia syndrome virus
HSV-1	Herpes simples virus 1
hpi	Hours post infection
Rac1	Ras-related C3 botulinum toxin substrate 1
$2A^{pro}$	2A protease
LC3/MAP1LC3B	Microtubule associated protein 1 light chain 3 beta
P62/SQSTM1	Sequestosome 1
DNMT1	DNA methyltransferase 1

Supplementary Information

The online version contains supplementary material available at https://doi.org/10.1186/s12866-025-03752-8.

Supplementary Material 1

Supplementary Material 2

Acknowledgements

We thank Professor Jianguo Wu of Jinan University for providing the plasmids expressing EV71 nonstructural proteins 2A–2B and 3AB–3D.

Author contributions

Q.Y., J.W., D.C, Y.L., F.Z.: conceptualization, methodology, software, data curation and writing-original draft. R.L., Y.C., N.J., Y.H.: methodology, data curation and visualization. Z.W.: administration of the research activity, funding the project, reviewing and editing the manuscript. All authors critically reviewed the manuscript and approved the final version.

Funding

This work was supported by the National Natural Science Foundation of China (U22A20335 and 31970149 to W.Z.W, 81900823 to C.D.Y); the Major Research and Development Project (2018ZX10301406 to W.Z.W.) and Nanjing University-Ningxia University Collaborative Project (2017BN04 to W.Z.W.).

Data availability

The datasets used and/or analyzed during the current study are available from the corresponding author on reasonable request.

Declarations

Ethics approval and consent to participate
Not applicable.

Consent for publication
Not applicable.

Competing interests
The authors declare no competing interests.

Received: 7 September 2024 / Accepted: 8 January 2025
Published online: 29 January 2025

References

1. Yang F, Ren L, Xiong Z, et al. Enterovirus 71 outbreak in the people's Republic of China in 2008. J Clin Microbiol. 2009;47(7):2351–2.
2. Wu H, Xue M, Wu C, et al. Trend of hand, foot, and mouth disease from 2010 to 2021 and estimation of the reduction in enterovirus 71 infection after vaccine use in Zhejiang Province, China. PLoS ONE. 2022;17(9):e0274421.
3. Solomon T, Lewthwaite P, Perera D, Cardosa MJ, McMinn P, Ooi MH. Virology, epidemiology, pathogenesis, and control of enterovirus 71. Lancet Infect Dis. 2010;10(11):778–90.
4. Ooi MH, Wong SC, Lewthwaite P, Cardosa MJ, Solomon T. Clinical features, diagnosis, and management of enterovirus 71. Lancet Neurol. 2010;9(11):1097–105.
5. Zhu F, Xu W, Xia J, et al. Efficacy, safety, and immunogenicity of an enterovirus 71 vaccine in China. N Engl J Med. 2014;370(9):818–28.
6. Li R, Liu L, Mo Z, et al. An inactivated enterovirus 71 vaccine in healthy children. N Engl J Med. 2014;370(9):829–37.
7. Zhu FC, Meng FY, Li JX, et al. Efficacy, safety, and immunology of an inactivated alum-adjuvant enterovirus 71 vaccine in children in China: a multicentre, randomised, double-blind, placebo-controlled, phase 3 trial. Lancet. 2013;381(9882):2024–32.
8. Swain SK, Gadnayak A, Mohanty JN, Sarangi R, Das J. Does enterovirus 71 urge for effective vaccine control strategies? Challenges and current opinion. Rev Med Virol. 2022;32(4):e2322.
9. Li YP, Liang ZL, Gao Q, et al. Safety and immunogenicity of a novel human enterovirus 71 (EV71) vaccine: a randomized, placebo-controlled, double-blind, phase I clinical trial. Vaccine. 2012;30(22):3295–303.
10. Dean L. Thioguanine therapy and TPMT and NUDT15 genotype. In: Pratt VM, Scott SA, Pirmohamed M, Esquivel B, Kattman BL, Malheiro AJ, editors. Medical Genetics Summaries. Bethesda (MD): National Center for Biotechnology Information (US); 2012.
11. Bayoumy AB, Simsek M, Seinen ML, et al. The continuous rediscovery and the benefit-risk ratio of thioguanine, a comprehensive review. Expert Opin Drug Metab Toxicol. 2020;16(2):111–23.
12. Swaim CD, Perng YC, Zhao X et al. 6-Thioguanine blocks SARS-CoV-2 replication by inhibition of PLpro protease activities. bioRxiv: Preprint Serv Biology 2020.
13. Slaine PD, Kleer M, Duguay BA et al. Thiopurines activate an antiviral unfolded protein response that blocks influenza a virus glycoprotein accumulation. J Virol 2021.
14. Chen D, Liu Y, Zhang F, et al. 6-Thioguanine inhibits herpes Simplex Virus 1 infection of eyes. Microbiol Spectr. 2021;9(3):e0064621.
15. Jiang N, He Y, Wu J, et al. 6-Thioguanine inhibits severe fever with thrombocytopenia syndrome virus through suppression of EGR1. Antiviral Res. 2024;227:105916.
16. Maiuri MC, Zalckvar E, Kimchi A, Kroemer G. Self-eating and self-killing: crosstalk between autophagy and apoptosis. Nat Rev Mol Cell Biol. 2007;8(9):741–52.
17. Huang L, Yue J. The interplay of autophagy and enterovirus. Semin Cell Dev Biol. 2020;101:12–9.
18. Chen T, Tu S, Ding L, Jin M, Chen H, Zhou H. The role of autophagy in viral infections. J Biomed Sci. 2023;30(1):5.
19. Lee YR, Wang PS, Wang JR, Liu HS. Enterovirus 71-induced autophagy increases viral replication and pathogenesis in a suckling mouse model. J Biomed Sci. 2014;21(1):80.
20. Zhang C, Li Y, Li J. Dysregulated autophagy contributes to the pathogenesis of enterovirus A71 infection. Cell Biosci. 2020;10(1):142.
21. Chen D, Feng C, Tian X, Zheng N, Wu Z. Promyelocytic leukemia restricts Enterovirus 71 replication by inhibiting Autophagy. Front Immunol. 2018;9:1268.
22. Ji L, Yang E, He S, Jin Y, Chen D. Enterovirus 2 C protein suppresses IKKα phosphorylation by recruiting IKKβ and IKKα into viral inclusion bodies. Viral Immunol. 2021;34(4):218–26.
23. Wu J, You Q, Lyu R, et al. Folate metabolism negatively regulates OAS-mediated antiviral innate immunity via ADAR3/endogenous dsRNA pathway. Metabolism. 2023;143:155526.
24. Liu Y, You Q, Zhang F, Chen D, Huang Z, Wu Z. Harringtonine inhibits herpes simplex virus type 1 infection by reducing herpes virus entry mediator expression. Front Microbiol. 2021;12:722748.
25. Chen D, Wu J, Zhang F, et al. Trained immunity of intestinal tuft cells during infancy enhances host defense against enteroviral infections in mice. EMBO Mol Med. 2024;16(10):2516–38.
26. Wu J, Cai Y, Jiang N et al. Pralatrexate inhibited the replication of varicella zoster virus and vesicular stomatitis virus: an old dog with new tricks. Antiviral Res 2023:105787.
27. You Q, Wu J, Liu Y, et al. HMGB1 Release Induced by EV71 infection exacerbates blood-brain barrier disruption via VE-cadherin phosphorylation. Virus Res. 2023;338:199240.
28. Lyu R, Wu J, He Y, et al. Folate supports IL-25-induced tuft cell expansion following enteroviral infections. Faseb j. 2024;38(2):e23430.
29. Shang L, Xu M, Yin Z. Antiviral drug discovery for the treatment of enterovirus 71 infections. Antiviral Res. 2013;97(2):183–94.
30. Cox JA, Hiscox JA, Solomon T, Ooi MH, Ng LFP. Immunopathogenesis and Virus-Host Interactions of Enterovirus 71 in patients with Hand, Foot and Mouth Disease. Front Microbiol. 2017;8:2249.
31. Li ZH, Li CM, Ling P, et al. Ribavirin reduces mortality in enterovirus 71-infected mice by decreasing viral replication. J Infect Dis. 2008;197(6):854–7.
32. Shin JY, Wey M, Umutesi HG, Sun X, Simecka J, Heo J. Thiopurine Prodrugs Mediate Immunosuppressive effects by interfering with Rac1 protein function. J Biol Chem. 2016;291(26):13699–714.
33. Wang H, Li Y. Recent progress on Functional Genomics Research of Enterovirus 71. Virol Sin. 2019;34(1):9–21.
34. Calandria C, Irurzun A, Barco A, Carrasco L. Individual expression of poliovirus 2Apro and 3Cpro induces activation of caspase-3 and PARP cleavage in HeLa cells. Virus Res. 2004;104(1):39–49.
35. Li C, Qiao Q, Hao SB, et al. Nonstructural protein 2A modulates replication and virulence of enterovirus 71. Virus Res. 2018;244:262–9.
36. Gradzka S, Thomas OS, Kretz O, et al. Inhibitor of apoptosis proteins are required for effective fusion of autophagosomes with lysosomes. Cell Death Dis. 2018;9(5):529.
37. Hou P, Wang X, Wang H, et al. The ORF7a protein of SARS-CoV-2 initiates autophagy and limits autophagosome-lysosome fusion via degradation of SNAP29 to promote virus replication. Autophagy. 2023;19(2):551–69.
38. Pourianfar HR, Poh CL, Fecondo J, Grollo L. In vitro evaluation of the antiviral activity of heparan sulfate mimetic compounds against Enterovirus 71. Virus Res. 2012;169(1):22–9.
39. Zhang R, Chen J, Zi R, et al. Enterovirus 71-induced autophagosome fusion with multivesicular bodies facilitates viral RNA packaging into exosomes. Microb Pathog. 2022;173(Pt A):105875.
40. Li C, Huang L, Sun W, et al. Saikosaponin D suppresses enterovirus A71 infection by inhibiting autophagy. Signal Transduct Target Ther. 2019;4:4.
41. Lai JKF, Sam IC, Verlhac P et al. 2BC non-structural protein of Enterovirus A71 interacts with SNARE proteins to trigger autolysosome formation. Viruses 2017;9(7).
42. Al-Kuraishy HM, Jabir MS, Al-Gareeb AI, Saad HM, Batiha GE, Klionsky DJ. The beneficial role of autophagy in multiple sclerosis: yes or no? Autophagy. 2024;20(2):259–74.
43. Zhang D, An X, Li Q, et al. Thioguanine induces apoptosis in Triple-negative breast Cancer by regulating PI3K-AKT pathway. Front Oncol. 2020;10:524922.
44. Puto LA, Reed JC. Daxx represses RelB target promoters via DNA methyltransferase recruitment and DNA hypermethylation. Genes Dev. 2008;22(8):998–1010.
45. Yuan B, Zhang J, Wang H, et al. 6-Thioguanine reactivates epigenetically silenced genes in acute lymphoblastic leukemia cells by facilitating proteasome-mediated degradation of DNMT1. Cancer Res. 2011;71(5):1904–11.
46. Aponte-Diaz D, Vogt MR, Cameron CE. An unexpected, pH-sensitive step of the enterovirus D68 lifecycle. mBio. 2023;14(6):e0228123.

47. Galitska G, Jassey A, Wagner MA, Pollack N, Miller K, Jackson WT. Enterovirus D68 capsid formation and stability requires acidic compartments. mBio. 2023;14(5):e0214123.
48. Tang F, Xia H, Wang P, et al. The identification and characterization of nucleic acid chaperone activity of human enterovirus 71 nonstructural protein 3AB. Virology. 2014;464–465:353–64.
49. Yang W, Li D, Ru Y et al. Foot-and-Mouth Disease Virus 3A protein causes Upregulation of Autophagy-Related protein LRRC25 to inhibit the G3BP1-Mediated RIG-Like helicase-signaling pathway. J Virol 2020;94(8).
50. Zhang Y, Yao L, Xu X, et al. Enterovirus 71 inhibits cytoplasmic stress granule formation during the late stage of infection. Virus Res. 2018;255:55–67.

Publisher's note